UC Berkeley
UC Berkeley Previously Published Works

Title
Relationship between Ion Transport and Phase Behavior in Acetal-Based Polymer Blend Electrolytes Studied by Electrochemical Characterization and Neutron Scattering

Permalink
https://escholarship.org/uc/item/5dx9f9vb

Journal
Macromolecules, 55(24)

ISSN
0024-9297

Authors
Lee, Jaeyong
Gao, Kevin W
Shah, Neel J
et al.

Publication Date
2022-12-27

DOI
10.1021/acs.macromol.2c01724

Peer reviewed

eScholarship.org Powered by the California Digital Library
University of California

Macromolecules

pubs.acs.org/Macromolecules Article

Relationship between Ion Transport and Phase Behavior in Acetal-Based Polymer Blend Electrolytes Studied by Electrochemical Characterization and Neutron Scattering

Jaeyong Lee, Kevin W. Gao, Neel J. Shah, Cheol Kang, Rachel L. Snyder, Brooks A. Abel, Lilin He, Susana C. M. Teixeira, Geoffrey W. Coates, and Nitash P. Balsara*

Cite This: *Macromolecules* 2022, 55, 11023−11033 Read Online

ACCESS | Metrics & More | Article Recommendations | Supporting Information

Downloaded via UNIV OF CALIFORNIA BERKELEY on May 9, 2023 at 16:56:09 (UTC).
See https://pubs.acs.org/sharingguidelines for options on how to legitimately share published articles.

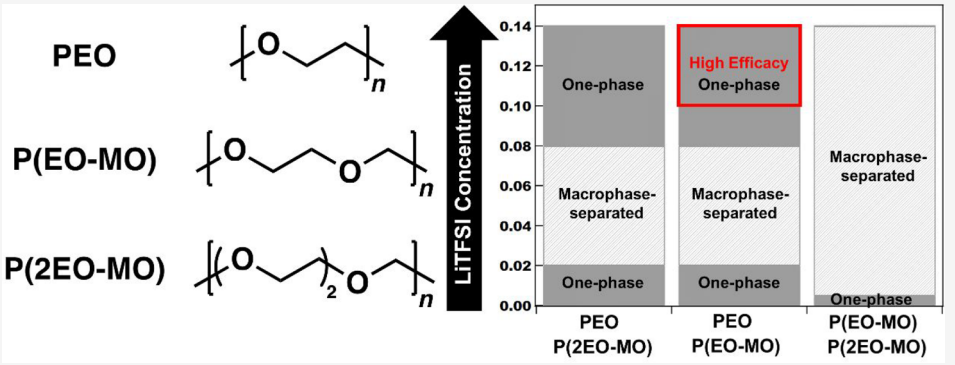

ABSTRACT: We have studied ion transport in electrolytes created by blending two different polymers and lithium bis(trifluoromethanesulfonyl)imide (LiTFSI). The polymers covered in this study are poly(ethylene oxide) (PEO), poly(1,3,6-trioxocane) (P(2EO-MO)), and poly(1,3-dioxolane) (P(EO-MO)). Ion transport is quantified by the product $\kappa\rho_+$ which is defined as the efficacy of the electrolytes, where κ is conductivity and ρ_+ is the current fraction determined by the Bruce−Vincent method. Polymer blends can be either one-phase or macrophase-separated. We used small-angle neutron scattering (SANS) to distinguish between these two possibilities. The random phase approximation (RPA) was used to interpret SANS data from one-phase blends. The effect of added salt on polymer blend thermodynamics is quantified by an effective Flory−Huggins interaction parameter. All polymer blends were one-phase in the absence of salt. Adding salt in small concentrations results in macrophase separation in all cases. One-phase systems were observed in the PEO/P(EO-MO)/LiTFSI blends at high salt concentrations. In most of the polymer blend electrolytes, the measured $\kappa\rho_+$ was either lower than or comparable to that of the homopolymer electrolytes. An exception to this was one-phase PEO/P(EO-MO)/LiTFSI blends electrolytes at high salt concentrations.

INTRODUCTION

Polymer electrolytes are our current interest as they can replace the flammable organic solvents used in current rechargeable lithium batteries.[1−4] While large varieties of mixtures of diverse polymers and different lithium salts have been studied,[5−11] poly(ethylene oxide) (PEO) mixed with lithium bis(trifluoromethanesulfonyl)imide (LiTFSI) continues to serve as a standard in the field.[12−16] Ionic conductivity, κ, is an important parameter but it reflects the motion of both cations and anions. While the conductivity of PEO/LiTFSI mixtures is reasonably high at elevated temperatures such as 90 °C, it is dominated by the motion of anions.[16] The performance of electrolytes in lithium batteries depends on the mobility of lithium cations, and an approach for evaluating this was developed by Bruce, Vincent, and Watanabe et al.[17,18] In this method, a potential is applied across a lithium symmetric cell and one measures the current fraction, ρ_+, defined as a ratio of the final (steady-state) to the initial current, which relates the amount of current carried by the cation.[19−24] In the limit of small applied currents, the efficacy of electrolytes is related to the product $\kappa\rho_+$. Unfortunately, the value of ρ_+ of PEO/LiTFSI mixtures is relatively low; at the salt concentration where κ is maximized, ρ_+ is only about 0.08. While there are a few recent reports of promising electrolytes with high values of κ and ρ_+,[25] the challenge of designing electrolytes with $\kappa\rho_+$ values higher than that of PEO/LiTFSI is significant.[26] In most polymers, efforts to increase ρ_+ led to a disproportionate decrease in κ.[27−29]

Received: August 18, 2022
Revised: November 15, 2022
Published: December 12, 2022

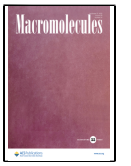

© 2022 American Chemical Society

https://doi.org/10.1021/acs.macromol.2c01724
Macromolecules 2022, 55, 11023−11033

The purpose of this study is to examine the possibility of obtaining polymer electrolytes with high $\kappa\rho_+$ values by blending two polymers. Conventional liquid electrolytes for lithium batteries are blends of two organic solvents and a salt. One of the organic solvents is a high dielectric constant liquid such as ethylene carbonate (EC), while the other is a low dielectric constant liquid such as dimethyl carbonate (DMC).[30,31] Ion dissociation is enabled by a high dielectric constant liquid, but these solutions would be extremely viscous if the low dielectric solvent were absent. In fact, EC is a solid at room temperature. Given that PEO is a polymer with a low dielectric constant, we investigated blending it with a more polar polymer, poly(1,3-dioxolane) P(EO-MO).[32] In a previous publication, we studied polymer blend electrolytes comprising PEO, poly(1,3,6-trioxocane) P(2EO-MO), and LiTFSI.[33] In this study, we examined both PEO/P(EO-MO)/LiTFSI and P(EO-MO)/P(2EO-MO)/LiTFSI blends. The blend components of interest are given in Scheme 1. Small-angle neutron scattering (SANS) is used to study the phase behavior of these blends. We also present electrochemical data showing that the $\kappa\rho_+$ values of several of our blends are somewhat higher than those of PEO/LiTFSI. The subject of polymer blend electrolytes has been studied by other groups.[34−37] We review these studies in the Results and Discussion section, after we present data from the systems listed above.

Scheme 1. Chemical structure of poly(ethylene oxide) (PEO), poly(1,3-dioxolane) (P(EO-MO)), poly(1,3,6-trioxocane) (P(2EO-MO)), and lithium bis(trifluoromethanesulfonyl)imide (LiTFSI)

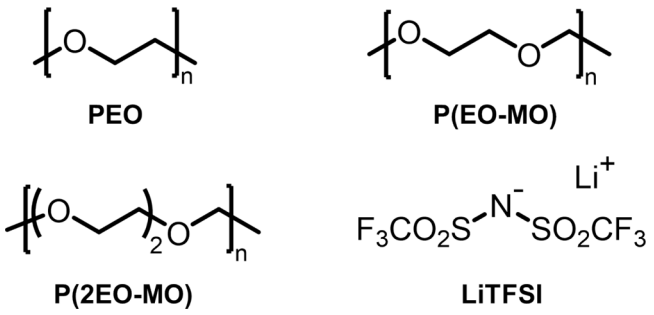

MATERIALS AND METHODS

Polymer Blend Electrolyte Preparation and Composition. The molar masses, M_n, and dispersities, $Đ$, of PEO (Polymer Source), deuterated PEO (dPEO) (Polymer Source), P(EO-MO) (synthesized as described in ref 32), P(2EO-MO), and deuterated P(EO-MO) (dP(EO-MO)) (synthesized as described in the Supporting Information) used in this study are summarized in Table 1.

Electrolytes used for SANS experiments were dPEO/P(EO-MO)/LiTFSI and dP(EO-MO)/P(2EO-MO)/LiTFSI blends. Electrochemical measurements were also performed on PEO/P(EO-MO)/LiTFSI and P(EO-MO)/P(2EO-MO)/LiTFSI blends (no deuterated polymers). All polymers were dried in a glovebox antechamber under vacuum at 90 °C for at least 24 h prior to use. LiTFSI was dried under vacuum at 120 °C for at least 72 h. The polymer composition of the blends was 50/50 by weight. Blends were created by mixing the required amounts of polymers and salt in acetonitrile. The electrolytes were prepared by evaporating the acetonitrile on a hot plate in a glovebox at 80 °C overnight. This was followed by a final drying step in the glovebox antechamber under vacuum at 90 °C for 24 h. The salt concentration of the blends was quantified by the molar ratio of Li atoms in the salt to O atoms in the polymers ($r = \frac{[Li]}{[O]}$), calculated as in ref 33. Electrolyte r values ranged from 0 to 0.14.

Table 1. Molar Masses and Dispersities of Homopolymers, and Type of Experiments Used in This Study

Polymer	M_n (kg mol^{-1})	$Đ$	Experiments
dPEO	35	1.09	SANS
P(EO-MO)	25	1.69	Electrochemical Measurements/ SANS
PEO	35	1.08	Electrochemical Measurements
dP(EO-MO)	22	1.79	SANS
P(2EO-MO)	21	1.58	Electrochemical Measurements/ SANS
P(EO-MO)	18	1.86	Electrochemical Measurements

SANS Sample Preparation and Experiment. Sample preparation for SANS experiments was conducted following procedures outlined previously.[38]

SANS experiments on dPEO/P(EO-MO)/LiTFSI blends were conducted on the NG7SANS beamline at the National Institute of Standards and Technology Center for Neutron Research.[39] Measurements were performed with a neutron wavelength of 6 Å and up to three sample-to-detector distances (SDDs) of 13, 4, and 1 m. The shortest distance, 1 m, was used with a detector offset of 25 cm to extend the scattering angle (2θ) attainable. Overall, the three configurations allowed for access to a scattering wave-vector magnitude, $q = \frac{4\pi}{\lambda}\sin(\theta)$, ranging from 0.03 to 5.5 nm^{-1}. The neutron beam size was defined by a 9.5 × 10^{-3} cm aperture. Data were collected at 20 °C increments between 70 and 110 °C. All measurements were reversible and repeatable upon either heating or cooling. Samples were equilibrated for at least 30 min at each temperature. A 9-position Peltier cooling/heating sample changer block was used to drive and maintain constant sample temperature. Samples of thickness of 1 mm were used. Data were reduced using the data reduction software package for IGOR provided by the NIST Center for Neutron Research.[40] The total scattering intensity was corrected for detector sensitivity, background, and empty cell contributions as well as sample transmission and thickness.[40,41]

SANS experiments on dP(EO-MO)/P(2EO-MO)/LiTFSI blends were conducted on the HFIR GP-SANS CG-2 beamline at Oak Ridge National Laboratory.[42] Measurements were performed with a neutron wavelength of 6 Å and three SDDs of 19, 6, and 1 m. Overall, the three configurations allowed for access to q ranging from 0.03 to 5.5 nm^{-1}. The neutron beam size was defined by a 12 mm diameter sample aperture. Data were collected at 20 °C increments between 70 and 110 °C. All measurements were reversible and repeatable upon either heating or cooling. Samples were equilibrated for at least 30 min at each temperature. A 12-position Peltier cooling/heating sample changer block was used to drive and maintain constant sample temperature. The samples thickness was 1 mm. Data were reduced using a software package in Jupyter provided by the Oak Ridge National Laboratory.[43] The total scattering intensity was corrected for detector sensitivity, background, and empty cell contributions as well as sample transmission and thickness. The intensity was placed on an absolute scale using a previously calibrated porous silica secondary standard.[42]

Electrochemical Sample Preparation and Experiments. Polymer blend electrolytes were made by the procedure described above. All blends contained equal mass of the two polymers. Because we used hydrogenated polymers for these experiments, the volume fractions of polymers in these samples were slightly different from those used in SANS experiments. The compositions of all electrolytes are given in Table S1. Electrochemical experiments were conducted on the blends using two types of cells as described in ref 44. κ was measured using blocking stainless steel electrodes. ρ_+ was measured using nonblocking lithium electrodes. Sample thickness was controlled using 380 and 500 μm thick silicone spacers for measuring κ and ρ_+, respectively. All experiments were conducted at 90 °C.

https://doi.org/10.1021/acs.macromol.2c01724
Macromolecules 2022, 55, 11023−11033

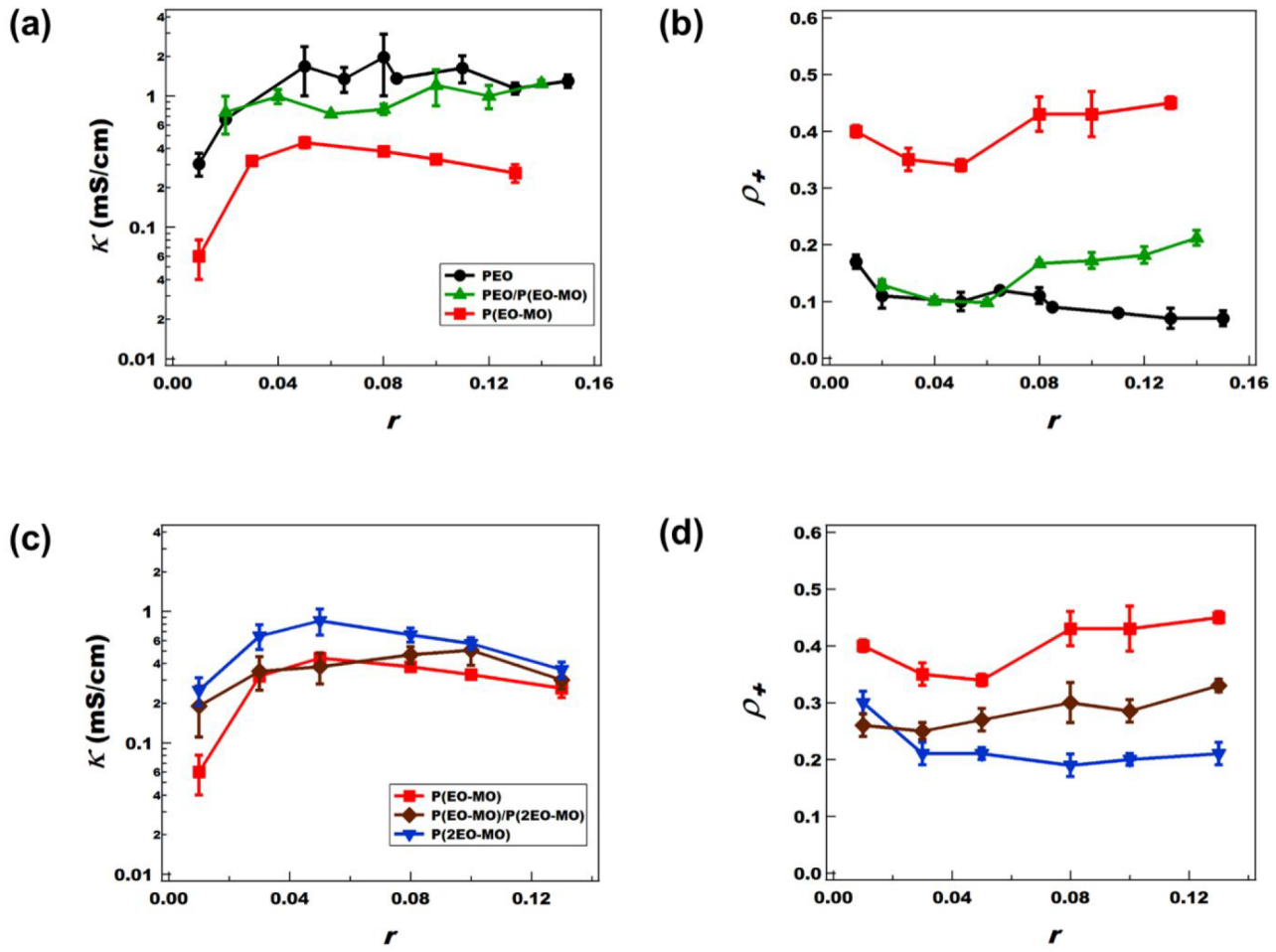

Figure 1. Electrochemical characterization of the PEO/P(EO-MO)/LiTFSI and P(EO-MO)/P(2EO-MO)/LiTFSI blend electrolytes as a function of LiTFSI concentration (r) compared with each homopolymer/LiTFSI (PEO: 35.0 kg mol^{-1}; P(EO-MO): 23.4 kg mol^{-1}; P(2EO-MO): 55.2 kg mol^{-1}) polymer electrolyte system from refs 32 and 33. (a), (c) Ionic conductivity (κ). (b), (d) Current fraction (ρ_+). Error bars represent the standard deviation of at least three measurements.

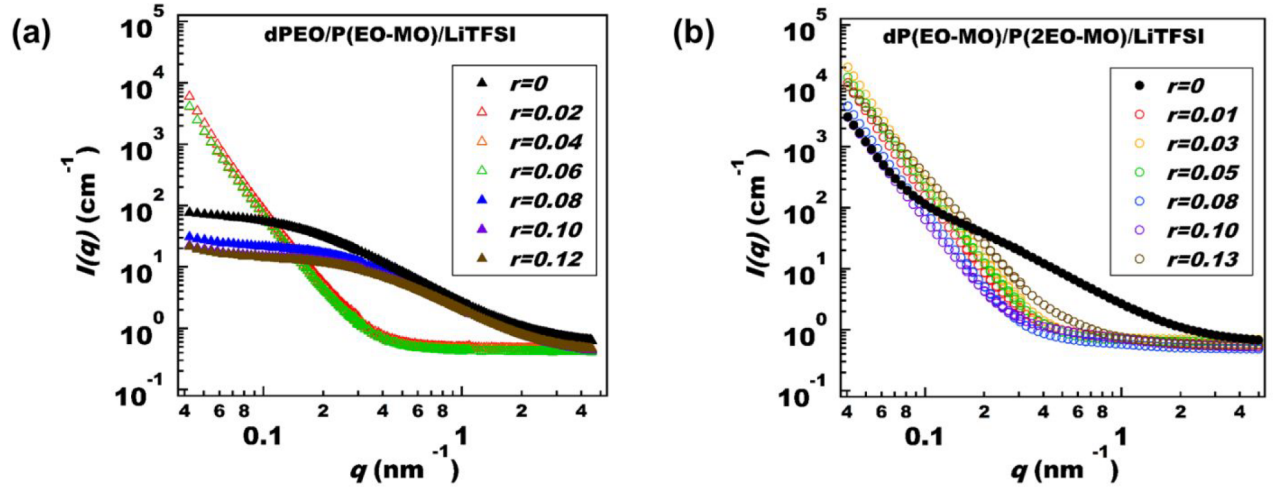

Figure 2. Measured absolute SANS intensity ($I(q)$) versus the magnitude of scattering vector (q) at 90 °C for (a) dPEO/P(EO-MO)/LiTFSI and (b) dP(EO-MO)/P(2EO-MO)/LiTFSI polymer blend electrolytes at different salt concentrations (r). Filled symbols correspond to one-phase electrolytes. Open symbols correspond to macrophase-separated electrolytes. Error bars represent one standard deviation of the scattering data and in most cases are smaller than the data points.

https://doi.org/10.1021/acs.macromol.2c01724
Macromolecules 2022, 55, 11023−11033

RESULTS AND DISCUSSION

Electrochemical characterization of all our polymer blend electrolytes as a function of salt concentration (r) is shown in Figure 1. The ionic conductivity (κ) of PEO/LiTFSI is about a factor of 3.8 or 5.1 higher than that of P(EO-MO)/LiTFSI at the same value of r. However, the ionic conductivity of the polymer blend electrolyte PEO/P(EO-MO)/LiTFSI is, however, similar to that of PEO at all values of r (Figure 1a). The current fraction (ρ_+) of PEO/LiTFSI is about a factor of 2.4 or 6.4 lower than that of P(EO-MO)/LiTFSI at the same value of r. However, the current fraction of the polymer blend electrolyte PEO/P(EO-MO)/LiTFSI is similar to that of PEO when $r < 0.08$. At higher r values, ρ_+ of the blend electrolyte is higher than that of PEO/LiTFSI; at $r = 0.14$, ρ_+ of the blend electrolyte is a factor of 3.0 higher. As described by the data in Figures 1a and 1b, the transport properties of the polymer blend electrolytes are not averages of values observed in the homopolymer electrolytes.

The ionic conductivity of P(2EO-MO)/LiTFSI is about a factor of 4.2 higher than that of P(EO-MO)/LiTFSI at $r = 0.01$ (Figure 1c). This factor decreases with increasing r; at $r = 0.13$, κ of P(2EO-MO)/LiTFSI is only 38% higher than that of P(EO-MO)/LiTFSI. At most r values, κ of the P(EO-MO)/P(2EO-MO)/LiTFSI polymer blend electrolytes lie between those of the homopolymer electrolytes, P(2EO-MO)/LiTFSI and P(EO-MO)/LiTFSI. The current fraction (ρ_+) of P(2EO-MO)/LiTFSI is about a factor of 2 lower than that of P(EO-MO)/LiTFSI at most the r values (Figure 1d). At most r values, ρ_+ of the P(EO-MO)/P(2EO-MO)/LiTFSI polymer blend electrolytes lie between those of the homopolymer electrolytes, P(2EO-MO)/LiTFSI and P(EO-MO)/LiTFSI.

The ion transport properties of polymer blend electrolytes will depend on whether the blends are one-phase or macrophase-separated. We note in passing that most pairs of high molecular weight polymers are immiscible with each other.[45,46] We conducted SANS experiments to determine the miscibility windows in our polymer blend electrolytes.

The measured absolute SANS intensity ($I(q)$) as a function of the magnitude of scattering vector (q) for the dPEO/P(EO-MO)/LiTFSI and dP(EO-MO)/P(2EO-MO)/LiTFSI polymer blends electrolytes is shown in Figure 2. We used the measured $I(q)$ in the q range 0.4 nm^{-1} < q < 1.0 nm^{-1} to determine if the electrolytes are one-phase or macrophase-separated. In principle, this could be determined by examining $I(q)$ in the limit $q \to 0$. However, the pure deuterated polymers exhibit strong scattering in this limit which may be due to impurities or voids, as noted in previous publications.[38,47−50] The scattering profiles of the pure deuterated polymers are given in Figure S5. The macrophase-separated dPEO/P(EO-MO)/LiTFSI blends show a sharp upturn of $I(q)$ below $q = 0.4$ nm^{-1}, when the salt concentration r is 0.02−0.06, as shown in Figure 2a. The macrophase-separated dP(EO-MO)/P(2EO-MO)/LiTFSI blends show a similar signature, but the sharp upturn of $I(q)$ is seen at q values ranging from 0.4 to 1.0 nm^{-1} when the salt concentration r is ≥0.01, as shown in Figure 2b. The lack of a sharp upturn of $I(q)$ in the q range noted above it is taken as a signature of a one-phase blend. In the absence of salt, both dPEO/P(EO-MO) and dP(EO-MO)/P(2EO-MO) blends are one-phase. Adding LiTFSI in dilute concentrations results in macrophase separation in both cases. At higher salt concentrations above $r = 0.08$, the dPEO/P(EO-MO)/LiTFSI blends become one-phase again. In contrast, the dP(EO-MO)/P(2EO-MO)/LiTFSI blends remain macrophase-separated in all salt concentrations studied.

We analyze the SANS data from homogeneous blends using the Flory−Huggins theory. In this theory, which applies to blends of two homopolymers

$$\frac{\Delta G_m}{k_B T} = \frac{\phi_1 \ln \phi_1}{N_1} + \frac{\phi_2 \ln \phi_2}{N_2} + \chi \phi_1 \phi_2 \quad (1)$$

where ΔG_m is the free energy of mixing per unit volume, k_B is the Boltzmann constant, T is the absolute temperature, labels 1 and 2 refer to the two polymers, ϕ_i is the volume fraction of component i, N_i is the number of repeat units in chain i, and χ is the Flory−Huggins interaction parameter between monomers of type 1 and 2.[51,52] N_1, N_2, and χ are based on a reference volume, $v = 0.1$ nm^3. The critical Flory−Huggins interaction parameter value, $\chi_{critical}$, is given by the following:

$$\chi_{critical} = \frac{1}{2}\left(\frac{1}{\sqrt{N_1}} + \frac{1}{\sqrt{N_2}}\right)^2 \quad (2)$$

Blends with $\chi < \chi_{critical}$ imply miscible phase, regardless of composition.

To account for added salt, we use a simple extension of eq 1.

$$\frac{\Delta G_m}{k_B T} = \phi_{polymer}\left(\frac{\phi_1 \ln \phi_1}{N_1} + \frac{\phi_2 \ln \phi_2}{N_2} + \chi_{eff} \phi_1 \phi_2\right) \quad (3)$$

where $\phi_{polymer}$ is the total polymer volume fraction and ϕ_i ($i = 1$ or 2) are the salt-free polymer volume fractions. The effect of added salt on thermodynamics is captured mainly by an effective Flory−Huggins parameter, χ_{eff}, which depends on salt concentration.[53−56] When $r \to 0$, $\phi_{polymer} \to 1$, eq 3 reduces to eq 1, and χ_{eff} reduces to the conventional χ parameter for polymer blends. After checking the qualitative phase behavior of the two blend systems as a function of r, we analyzed the $I(q)$ data to determine χ_{eff} as a function of blend composition. Before calculating χ_{eff}, the absolute SANS intensity was corrected for the contributions from coherent scattering of the deuterated chains and additional background scattering that includes the incoherent scattering from hydrogen atoms to obtain the absolute coherent SANS intensity from each blend, $I_{coh}(q)$[57]

$$I_{coh}(q) = I(q) - fI_{deuterated\ polymer/LiTFSI}(q) - I_{inc} \quad (4)$$

where f is the volume fraction of deuterated polymer which is calculated using eq 5.

$$f = \frac{\dfrac{w_1 + \dfrac{r n_1 w_1 M'_{salt}}{M'_1}}{\rho_1}}{\dfrac{w_1 + \dfrac{r n_1 w_1 M'_{salt}}{M'_1}}{\rho_1} + \dfrac{w_2 + \dfrac{r n_2 w_2 M'_{salt}}{M'_2}}{\rho_2}}, \quad (5)$$

Label 1 refers to the deuterated component, and label 2 refers to the nondeuterated polymer; w_i is the mass of component i, ρ_i is the mass density (ρ_{PEO} = 1.23 g cm^{-3}; ρ_{dPEO} = 1.34 g cm^{-3}; $\rho_{P(EO-MO)}$ = 1.32 g cm^{-3}; $\rho_{dP(EO-MO)}$ = 1.44 g cm^{-3}; $\rho_{P(2EO-MO)}$ = 1.32 g cm^{-3}; ρ_{LiTFSI} = 2.023 g cm^{-3}), M'_i is the monomer molar mass (M'_{EO} = 44.05 g mol^{-1}; M'_{EO-MO} = 68.05 g mol^{-1}; M'_{2EO-MO} = 118.05 g mol^{-1}; M'_{dPEO} = 48.05 g mol^{-1}; $M'_{dP(EO-MO)}$ = 74.03; M'_{salt} is 287.1 g mol^{-1}), and n_i is the number of oxygen atoms in each monomer (see Scheme 1). The

https://doi.org/10.1021/acs.macromol.2c01724
Macromolecules 2022, 55, 11023−11033

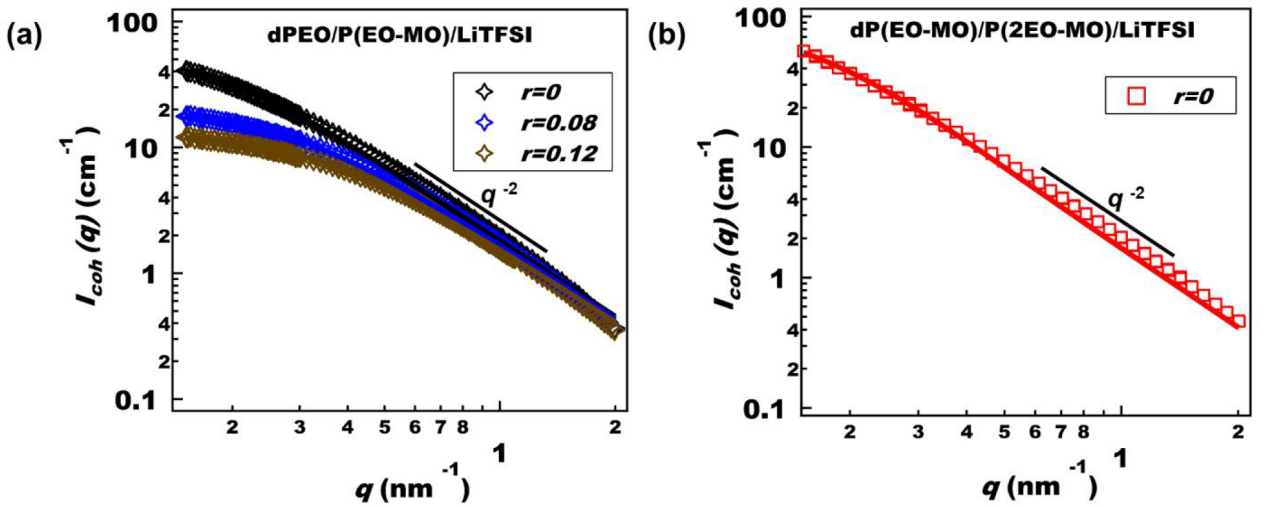

Figure 3. Coherent SANS intensity profiles ($I_{coh}(q)$) (open symbols) and corresponding RPA fits (solid curves) for one-phase blends at 90 °C. (a) dPEO/P(EO-MO)/LiTFSI blends and (b) dP(EO-MO)/P(2EO-MO). Error bars represent one standard deviation of the scattering data and in most cases are smaller than the data points.

densities reported above measured the value at 90 °C. All polymers are amorphous at this temperature. We assumed that the densities of P(2EO-MO) and P(EO-MO) are equal and that the volumes occupied by monomers of deuterated and nondeuterated polymers are identical. SANS profiles reflect scattering length density inhomogeneities which we assume are dominated by fluctuations in polymer concentration; we neglect the partitioning of salt across these fluctuations. $I_{\text{deuterated polymer/LiTFSI}}$ is the scattering from deuterated polymer/LiTFSI mixtures: $I_{\text{dPEO/LiTFSI}}$ was taken from ref 38, and $I_{\text{dP(EO−MO)/LiTFSI}}$ was measured (see the Supporting Information). I_{inc} is the incoherent scattering from hydrogen atoms which we estimate by fitting the measured SANS profile in the high q range 0.2 nm^{-1} < q < 5.0 nm^{-1}

$$I(q) = aP(q) + I_{\text{inc}} \tag{6}$$

where

$$P(q) = 2\left[\frac{\exp(-q^2R_d^2) - 1 + q^2R_d^2}{q^4R_d^4}\right] \tag{7}$$

a, I_{inc}, and R_d are fitting constants.[57] When the scattering from deuterated sample arises from heterogeneity in deuteration levels, the fitted parameter R_d is consistent with the radius of gyration of the polymer chains.[58] After subtracting $I_{\text{deuterated polymer/LiTFSI}}(q)$ and I_{inc} from $I(q)$, we obtain $I_{\text{coh}}(q)$ for miscible blends using eq 4. The results we obtained are shown in Figure 3.

Following ref 33, we use the following expression for analyzing $I_{\text{coh}}(q)$ from one-phase polymer blends based on the random phase approximation (RPA) method[59−63]

$$I_{\text{coh}}(q) = \phi_{\text{polymer}}(B_1 - B_2)^2 v\left(\frac{1}{S_{11}(q)} + \frac{1}{S_{22}(q)} - 2\chi_{\text{eff}}\right)^{-1} \tag{8}$$

where B_i is the coherent neutron scattering length density of component i, calculated as in ref 33 ($B_{\text{dPEO}} = 128.0 \times 10^{-15}$ mol cm^{-2}; $B_{\text{P(EO−MO)}} = 17.7 \times 10^{-15}$ mol cm^{-2}; $B_{\text{dP(EO−MO)}} = 139.0 \times 10^{-15}$ mol cm^{-2}; $B_{\text{P(2EO−MO)}} = 14.8 \times 10^{-15}$ mol cm^{-2}), v is reference volume (0.1 nm^3), and $S_{ii}(q)$ is the ideal structure factor of polymer i given by

$$S_{ii}(q) = \phi_i N_i P_i(q) \tag{9}$$

N_i is the number of repeat units in each polymer, given by

$$N_i = \frac{M_i}{\rho_i N_{\text{av}} v} \tag{10}$$

where N_{av} is Avogadro's number, M_i is the polymer molar mass (g mol^{-1}), ρ_i is the polymer density (g cm^{-3}), and $P_i(q)$ is the Debye function of the polymer i

$$P_i(q) = 2\left[\frac{\exp(-q^2R_{gi}^2 - 1 + q^2R_{gi}^2)}{q^4R_{gi}^4}\right],\quad R_{gi}^2 = \frac{N_i l_i^2}{6} \tag{11}$$

where R_{gi} is the radius of gyration of polymer i and l_i is the statistical segment length of polymer i. We assumed that the l_i value of PEO is 0.58 nm.[38] The nominal values for l_i of P(EO-MO) and P(2EO-MO) were taken to be 0.58 nm. Equations 8−11 apply to one-phase blends of monodisperse polymers wherein the ions are distributed homogeneously. The scattering data in Figure 3 were fitted to eq 8 with two adjustable parameters: χ_{eff} and α where the values of l_i of P(EO-MO) and P(2EO-MO) were also assumed to be 0.58α nm (α is constant). The parameter α accounts for differences in the statistical segment lengths of the polymers (PEO, P(EO-MO), and P(2EO-MO)) in the blends. It reflects the average distortion of chains in the blends. α is generally greater than 1 for all blends. We attribute to the increased stiffness of P(EO-MO) or P(2EO-MO) chains relative to that of the PEO chains. α was found to be a weak function of temperature. To minimize errors in fitting, we used a temperature-average value of α for each miscible blend (70, 90, and 110 °C; see the Supporting Information). The final fits were obtained with χ_{eff} as the only adjustable parameter. The blend compositions and α parameters obtained using RPA fitting are listed in Table 2. The curves in Figure 3 show those fits from which we estimate χ_{eff} for all one-phase polymer blends. $I_{\text{coh}}(q)$ obtained from macrophase-separated blends could not be fit using this RPA-based approach (see Figure S7).

The temperature dependence of χ_{eff} of the miscible polymer blends, obtained by the fitting procedure described in the previous paragraph, is shown in Figure 4. The measured χ_{eff}

https://doi.org/10.1021/acs.macromol.2c01724
Macromolecules 2022, 55, 11023−11033

Table 2. Component Volume Fractions (ϕ_i)[a] and α Values of Miscible Blends

polymer blend	ϕ_1	ϕ_2	$\phi_{polymer}$	α
dPEO/P(EO-MO) (r = 0)	0.50	0.50	1.00	1.37 ± 0.03
dPEO/P(EO-MO) (r = 0.08)	0.50	0.50	0.72	1.17 ± 0.03
dPEO/P(EO-MO) (r = 0.10)	0.50	0.50	0.67	1.15 ± 0.01
dPEO/P(EO-MO) (r = 0.12)	0.50	0.50	0.63	1.14 ± 0.01
dP(EO-MO)/P(2EO-MO) (r = 0)	0.52	0.48	1.00	1.46 ± 0.01

[a] ϕ_1: volume fraction of deuterated polymer; ϕ_2: volume fraction of nondeuterated polymer.

values have not been corrected for the dispersity of polymer chains or the possibility of salt partitioning. We fit this dependence to the function of the form

$$\chi_{eff} = \frac{A}{T} + B \tag{12}$$

where A and B are constants.[64] These constants are given in Table 3. As shown in Figure 4a, χ_{eff} of dPEO/P(EO-MO) (r = 0) decreases slightly with increasing T. The value of B for the system is small, $(8.5 \pm 0.4)\ 10^{-3}\ K^{-1}$. Also shown in Figure 4a is $\chi_{critical}$ calculated using eq 2. We assume the χ_{eff} for macrophase-separated systems exceeds $\chi_{critical}$. Adding salt to this blend results in macrophase separation at salt concentrations up to r = 0.06. We conclude that χ_{eff} of dPEO/P(EO-MO)/LiTFSI blends with $0.02 < r < 0.06$ is greater than $\chi_{critical}$ (5.2×10^{-3}). Further increasing the salt concentration to r = 0.08 results in a one-phase blend wherein χ_{eff} that decreases significantly with increasing T. The value of B for the system is large, $(71 \pm 3) \times 10^{-3}\ K^{-1}$. The χ_{eff} values of dPEO/P(EO-MO)/LiTFSI blends at r = 0.10 and 0.12 also decrease with increasing T but exhibit smaller values of B (see Table 3). As shown in Figure 4b, χ_{eff} of dP(EO-MO)/P(2EO-MO) (r = 0) increase slightly with increasing T. The value of B for the system is small but negative, $(-1.6 \pm 0.7) \times 10^{-3}\ K^{-1}$. Adding salt results in macrophase separation at all values of r between 0.01 and 0.13. In this window, χ_{eff} is greater than $\chi_{critical}$ (7.7×10^{-3}).

Figure 5a shows the dependence of χ_{eff} on r for the dPEO/P(EO-MO)/LiTFSI blends at different temperatures. At low salt concentrations ($0.02 \le r \le 0.06$), we only get a lower bound for χ_{eff} which is $\chi_{critical}$. We thus only present the lower bounds of the error bars for χ_{eff} in this salt concentration window. At higher salt concentrations, χ_{eff} generally decreases with increasing salt concentration. It is evident that χ_{eff} of dPEO/P(EO-MO)/LiTFSI blends is a nonmonotonic function of r. This can be explained as a competition between ion solvation and entropic effects. At low salt concentrations, ion solvation effect is dominate; a model for this effect was proposed by Wang.[65] At high salt concentrations, entropic contributions from the dissociation of ions are dominant,[66] and this results in a reduction of χ_{eff}.

Table 3. A and B (K^{-1}) Values for dPEO/P(EO-MO)/LiTFSI and dP(EO-MO)/P(2EO-MO) Blends at Various r

polymer blend	A	$B \times 10^{-3}$ (K^{-1})
dPEO/P(EO-MO) (r = 0)	−2.2 ± 0.1	8.5 ± 0.4
dPEO/P(EO-MO) (r = 0.08)	−26 ± 1	71 ± 3
dPEO/P(EO-MO) (r = 0.10)	−14 ± 1	34 ± 1
dPEO/P(EO-MO) (r = 0.12)	−3.6 ± 0.1	6.3 ± 0.2
dP(EO-MO)/P(2EO-MO) (r = 0)	2.6 ± 0.3	−1.6 ± 0.7

We have very limited information about the dependence of χ_{eff} on r for the dP(EO-MO)/P(2EO-MO)/LiTFSI blends, as shown in Figure 5b. In these blends, we only conclude χ_{eff} increases above $\chi_{critical}$ when r increases from 0 to 0.01.

We now discuss the relationship between the electrochemical properties of the polymer blend electrolyte and the blend phase behavior. Under a small applied potential gradient, the dc current is proportional to the product $\kappa\rho_+$. We thus refer to $\kappa\rho_+$ as the efficacy of electrolyte. In Figure 6a, we plot $\kappa\rho_+$ as a function of r for three systems: PEO/LiTFSI, P(EO-MO)/LiTFSI, and PEO/P(EO-MO)/LiTFSI blends. The dependence of $\kappa\rho_+$ of PEO/LiTFSI and P(EO-MO)/LiTFSI on r is similar, within experimental error. Given this fact, one might expect the dependence of $\kappa\rho_+$ of PEO/P(EO-MO)/LiTFSI blends on r to be similar to that of the homopolymer electrolytes. Figure 6a shows that this is not the case. At r = 0.05, $\kappa\rho_+$ of polymer blend electrolytes is 0.08 mS/cm while that of the homopolymer electrolytes is 0.16 mS/cm. In contrast, at r =

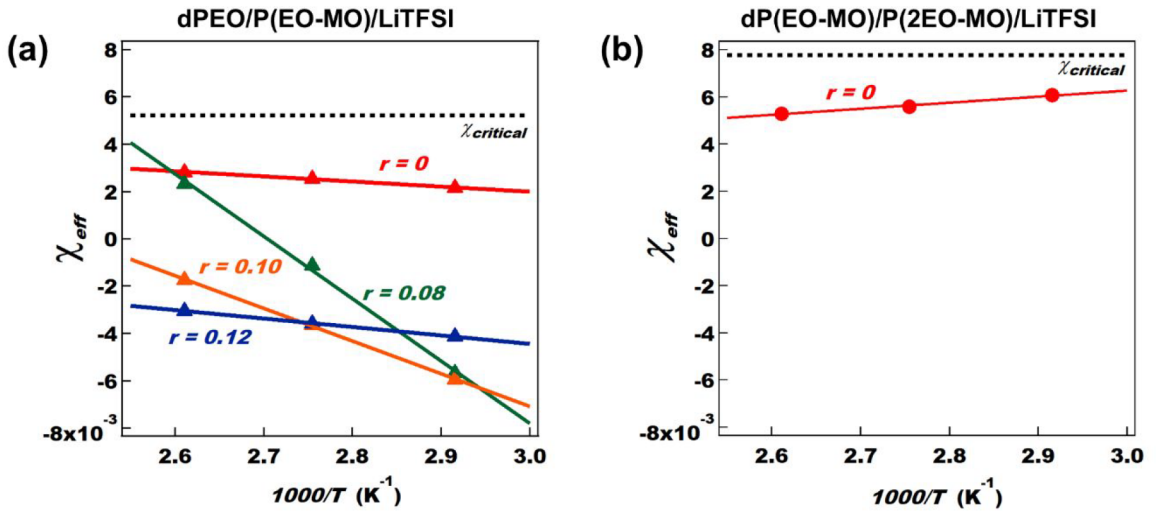

Figure 4. Effective Flory–Huggins interaction parameter (χ_{eff}) as a function of inverse temperature ($1/T$) for the one-phase (a) dPEO/P(EO-MO)/LiTFSI polymer blend electrolytes and (b) dP(EO-MO)/P(2EO-MO) polymer blends. All dP(EO-MO)/P(2EO-MO)/LiTFSI blends were macrophase-separated. $\chi_{critical}$ is calculated by eq 2. Error bars represent one standard deviation of the χ_{eff} fits and are smaller than the symbols.

https://doi.org/10.1021/acs.macromol.2c01724
Macromolecules 2022, 55, 11023−11033

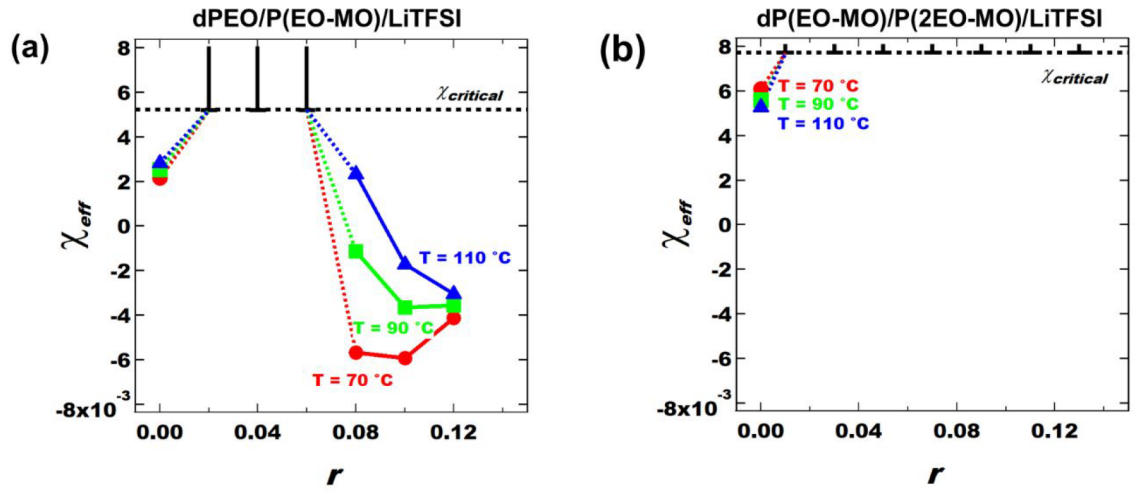

Figure 5. Effective Flory–Huggins interaction parameter (χ_{eff}) as a function of salt concentration, r, for the dPEO/P(EO-MO)/LiTFSI and dP(EO-MO)/P(2EO-MO)/LiTFSI polymer blend electrolytes at different temperatures. The symbols represent measured values of χ_{eff} at salt concentrations and temperatures where the blends are homogeneous. (a) In the salt concentration range, $0.02 \leq r < 0.08$, we can only determine the lower bound of the error bar for χ_{eff} of dPEO/P(EO-MO)/LiTFSI due to macrophase separation. (b) dP(EO-MO)/P(2EO-MO)/LiTFSI polymer blends are macrophase-separated at all salt concentrations and temperatures. $\chi_{critical}$ is calculated by eq 2. Error bars represent one standard deviation of the χ_{eff} fits and are smaller than the symbols.

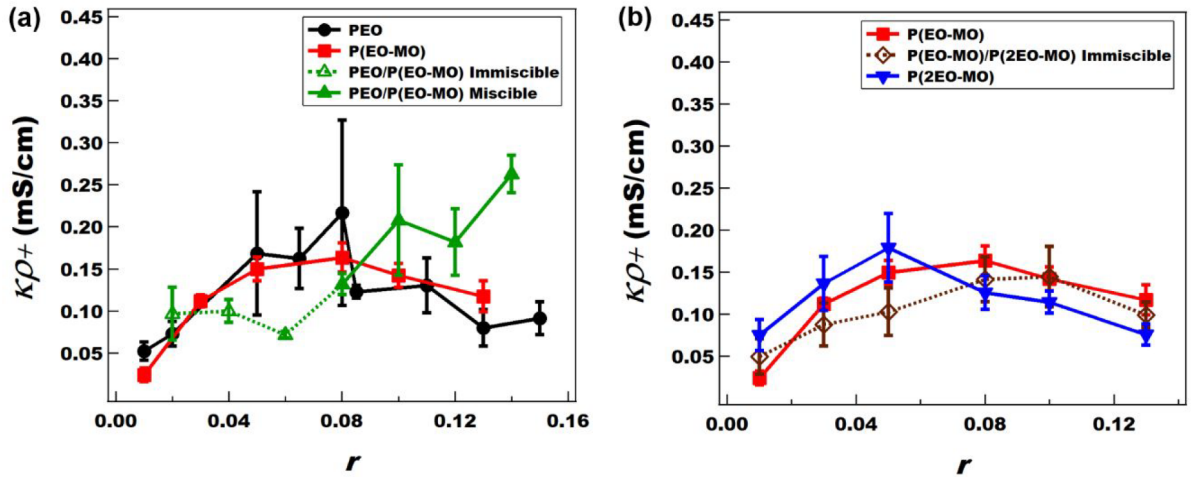

Figure 6. Efficacy, $\kappa\rho_+$, of PEO/P(EO-MO)/LiTFSI and P(EO-MO)/P(2EO-MO)/LiTFSI polymer blend electrolytes as a function of r compared to each homopolymer/LiTFSI (PEO: 35.0 kg mol^{-1}; P(EO-MO): 23.4 kg mol^{-1}; P(2EO-MO): 55.2 kg mol^{-1}) at 90 °C. Homopolymer/LiTFSI data were collected from refs 32 and 33. Solid lines imply one-phase systems, and dashed lines imply macrophase-separated systems. Error bars represent the standard deviation of at least three measurements.

0.14, $\kappa\rho_+$ of polymer blend electrolytes is 0.26 mS/cm while that of the homopolymer electrolytes is 0.10 mS/cm. The main difference between the two chosen r values is their phase behavior: the polymer blend electrolyte at $r = 0.14$ is one-phase, while the polymer blend electrolyte at $r = 0.05$ is macrophase-separated. It is evident that one-phase polymer blend electrolytes can exhibit efficacies that are higher than homopolymer electrolytes. For completeness, in Figure 6b, we plot $\kappa\rho_+$ as a function of r for three systems: P(EO-MO)/LiTFSI, P(2EO-MO)/LiTFSI, and P(EO-MO)/P(2EO-MO)/LiTFSI blends. The dependence of $\kappa\rho_+$ on r is similar for all three systems. All of the polymer blend electrolytes in Figure 6b are macrophase-separated.

Finally, we compare our findings with literature on polymer blend electrolytes. Theoretical work by Wheatle et al.[35] shows that conductivity of polymer blend electrolytes can be higher than that of homopolymer electrolytes, especially if the polarities of the blended polymers are different and the blend is one-phase. In the simulations, the conductivity of macrophase-separated blends was systematically lower than the average conductivity of the two homopolymer electrolytes. Our experimental data on macrophase-separated blends are consistent with this result (see Figures 1a,c). In experimental work, Caradant et al.[36] studied the conductivity of PEO blended with polymers with different polarities, including polycarprolactone (PCL), polypropylene carbonate (PPC), and polyvinylpyrrolidone (PVP). All of the blends in this study were macrophase-separated and exhibited lower conductivity as compared with PEO electrolytes. To our knowledge, Figure 6a is the only data set in the literature thus far that shows higher efficacy of a polymer blend electrolyte relative to PEO. We speculate that the difference in polarity between P(EO-MO) and PEO is responsible for the higher efficacy as predicted by Wheatle et al. We note, however, that higher efficacy was not obtained at low salt concentrations ($r < 0.10$).

https://doi.org/10.1021/acs.macromol.2c01724
Macromolecules 2022, 55, 11023−11033

Further work is needed to establish the dependence of the efficacy of polymer blend electrolytes on salt concentration.

CONCLUSION

In this study, we have examined the possibility of optimizing ion transport in polymer electrolytes by blending two different polymers blends. The polymers covered in this study are PEO, P(2EO-MO), and P(EO-MO). LiTFSI is added to the polymers to create electrolytes. The properties of PEO/P(2EO-MO)/LiTFSI blends were reported in ref 33. The properties of PEO/P(EO-MO)/LiTFSI and P(EO-MO)/P(2EO-MO)/LiTFSI are reported in this paper. Ion transport is quantified by the product $\kappa\rho_+$ which is defined as the efficacy of the electrolytes. Polymer blends can be either one-phase or macrophase-separated. We used SANS to distinguish between two possibilities and the results thus obtained are summarized in Figure 7. In addition, SANS from one-phase systems was analyzed to obtain χ_{eff}. Our analysis is based on a simple model that ignores the partitioning of salt in polymer concentration fluctuations and polydispersity effects. We hope to develop more complete models in the future. All polymer blends were one-phase in the absence of salt. Adding salt in small concentration results in macrophase separation in all cases. One-phase systems were obtained in the two blends containing PEO at high salt concentrations ($r \geq 0.08$). The boundaries between one-phase and macrophase-separated systems is assumed to be at the average value of r where the two types of system were observed. In most of the polymer blend electrolytes, the measured $\kappa\rho_+$ was either lower than or comparable to that of the homopolymer electrolytes. An exception to this was one-phase PEO/P(EO-MO)/LiTFSI blends electrolytes with $r \geq 0.10$, as shown in Figure 7. The molecular underpinnings of both thermodynamic and ion transport properties remain to be established.

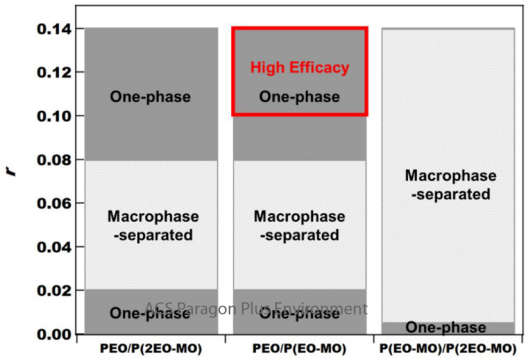

Figure 7. Summary of phase behavior and ion transport efficacy, $\kappa\rho_+$, of polymer blend electrolytes with added LiTFSI salt at 90 °C. We distinguish between one-phase and macrophase-separated blends. The red box identifies one-phase systems with efficacies higher than that of homopolymer electrolytes.

ASSOCIATED CONTENT

Supporting Information

The Supporting Information is available free of charge at https://pubs.acs.org/doi/10.1021/acs.macromol.2c01724.

Synthesis and characteristics of deuterated P(EO-MO) and P(2EO-MO), Volume fraction for electrochemical property measurement, Absolute SANS scattering of deuterated dPEO/LiTFSI and dP(EO-MO)/LiTFSI, Coherent SANS scattering intensity of dPEO/P(EO-MO) and dP(EO-MO)/P(2EO-MO) at different temperatures, Analysis of macrophase-separated systems (PDF)

AUTHOR INFORMATION

Corresponding Author

Nitash P. Balsara − *Department of Chemical and Biomolecular Engineering, University of California, Berkeley, Berkeley, California 94720, United States; Materials Sciences Division, Lawrence Berkeley National Laboratory, Berkeley, California 94720, United States; Joint Center for Energy Storage Research (JCESR), Argonne National Laboratory, Lemont, Illinois 60439, United States;* orcid.org/0000-0002-0106-5565; Email: nbalsara@berkeley.edu

Authors

Jaeyong Lee − *Department of Chemical and Biomolecular Engineering, University of California, Berkeley, Berkeley, California 94720, United States; Materials Sciences Division, Lawrence Berkeley National Laboratory, Berkeley, California 94720, United States; Joint Center for Energy Storage Research (JCESR), Argonne National Laboratory, Lemont, Illinois 60439, United States;* orcid.org/0000-0001-9850-6525

Kevin W. Gao − *Department of Chemical and Biomolecular Engineering, University of California, Berkeley, Berkeley, California 94720, United States; Materials Sciences Division, Lawrence Berkeley National Laboratory, Berkeley, California 94720, United States; Joint Center for Energy Storage Research (JCESR), Argonne National Laboratory, Lemont, Illinois 60439, United States;* orcid.org/0000-0002-6794-1265

Neel J. Shah − *Department of Chemical and Biomolecular Engineering, University of California, Berkeley, Berkeley, California 94720, United States; Materials Sciences Division, Lawrence Berkeley National Laboratory, Berkeley, California 94720, United States;* orcid.org/0000-0002-2503-048X

Cheol Kang − *Joint Center for Energy Storage Research (JCESR), Argonne National Laboratory, Lemont, Illinois 60439, United States; Department of Chemistry and Chemical Biology, Cornell University, Ithaca, New York 14850, United States*

Rachel L. Snyder − *Joint Center for Energy Storage Research (JCESR), Argonne National Laboratory, Lemont, Illinois 60439, United States; Department of Chemistry and Chemical Biology, Cornell University, Ithaca, New York 14850, United States;* orcid.org/0000-0002-0569-0704

Brooks A. Abel − *Department of Chemistry, University of California, Berkeley, Berkeley, California 94720, United States;* orcid.org/0000-0002-2288-1975

Lilin He − *Neutron Scattering Division, Oak Ridge National Laboratory, Knoxville, Tennessee 37830, United States*

Susana C. M. Teixeira − *NIST Center for Neutron Research, National Institute of Standards and Technology, Gaithersburg, Maryland 20899, United States; Department of Chemical and Biomolecular Engineering, University of Delaware, Newark, Delaware 19716, United States*

Geoffrey W. Coates − *Joint Center for Energy Storage Research (JCESR), Argonne National Laboratory, Lemont, Illinois 60439, United States; Department of Chemistry and Chemical Biology, Cornell University, Ithaca, New York 14850, United States;* orcid.org/0000-0002-3400-2552

Complete contact information is available at:

https://pubs.acs.org/10.1021/acs.macromol.2c01724

Author Contributions

J.L. and K.W.G. contributed equally to this work.

Notes

The authors declare no competing financial interest.

■ ACKNOWLEDGMENTS

This work was intellectually led by the Joint Center for Energy Storage Research (JCESR), an Energy Innovation Hub funded by the U.S. Department of Energy, Office of Science, Office of Basic Energy Science, under Contract DE-AC02-06CH11357, which supported synthesis work conducted by C.K., R.L.S., and B.A.A. under the supervision of G.W.C. and characterization work conducted by J.L. and K.W.G. under the supervision of N.P.B. We acknowledge the Center for Neutron Science at the University of Delaware and funding under cooperative agreement #70NANB20H133 from NIST, U.S. Department of Commerce. This research used resources at the High Flux Isotope, a DOE Office of Science User Facility operated by the Oak Ridge National Laboratory. We acknowledge the support of the National Institute of Standards and Technology, U.S. Department of Commerce, in providing the neutron facilities used in this work. K.W.G. acknowledges funding from a National Defense and Science Engineering Graduate Fellowship. The statements, findings, conclusions and recommendations are those of the authors and do not necessarily reflect the view of NIST or the U.S. Department of Commerce. Certain commercial equipment, instruments, suppliers and software are identified in this paper to foster understanding. Such identification does not imply recommendation or endorsement by the National Institute of Standards and Technology, nor does it imply that the materials or equipment identified are necessarily the best available for the purpose.

■ LIST OF SYMBOLS

PEO, poly(ethylene oxide); P(2EO-MO), poly(1,3,6-trioxocane); P(EO-MO), poly(1,3-dioxolane); LiTFSI, lithium bis(trifluoromethanesulfonyl)imide; SANS, small-angle neutron scattering; 2EO-MO, 1,3,6-trioxocane; EO-MO, 1,3-dioxolane; M_n, number-average molar mass (kg mol^{-1}); $Đ$, dispersity; dPEO, deuterated poly(ethylene oxide); dP(EO-MO), deuterated poly(1,3-dioxolane); ϕ_i, volume fraction of component i; $\phi_{polymer}$, volume fraction of polymer components in a blend containing LiTFSI; w_i, weight of component i (g); w_{salt}, weight of LiTFSI salt (g); ρ_i, density of component i (g cm^{-3}); ρ_{salt}, density of LiTFSI salt (g cm^{-3}); r, molar ratio of lithium to oxygen atoms; M'_i, monomer molar mass of i (g mol^{-1}); M'_{salt}, molar mass of LiTFSI salt (g mol^{-1}); f, volume fraction of PEO and LiTFSI associated with PEO; SDD, sample-to-detector distance; θ, scattering angle; λ, wavelength (nm); q, magnitude of the scattering vector (nm^{-1}); $I(q)$, measured absolute SANS intensity (cm^{-1}); v, reference volume (nm^3); T, absolute temperature (K); N_i, number of repeat units per chain; $\chi_{critical}$, critical Flory−Huggins interaction parameter; χ_{eff}, effective Flory−Huggins interaction parameter; $I_{coh}(q)$, coherent scattering intensity (cm^{-1}); $I_{deuterated\ polymer/LiTFSI}(q)$, SANS intensity from deuterated polymer/LiTFSI mixtures (cm^{-1}); $I_{inc}(q)$, incoherent scattering intensity (cm^{-1}); $P_i(q)$, form factor; B_i, neutron scattering length density of component i (cm^{-2} mol^{-1}); b_i, neutron scattering length of component i (cm mol^{-1}); v_i, monomer molar volume of component i (cm^3 mol^{-1}); S_{ii}, structure factor; M_i, polymer molar mass of component i (g mol^{-1}); $R_{g,i}$, radius of gyration (cm); l_i, statistical segment length of component i (nm); α, RPA fitting parameter accounting for chain distortion; A, B, empirical constants for fitting χ; R^2, coefficient of determination; κ, ionic conductivity (S cm^{-1}); ρ_+, current fraction; $\kappa\rho_+$, efficacy (S cm^{-1}).

■ REFERENCES

(1) Goodenough, J. B.; Park, K.-S. The Li-Ion Reachargeable Battery: A Perspective. *J. Am. Chem. Soc.* **2013**, *135*, 1167−1176.
(2) Cheng, X.-B.; Zhang, R.; Zhao, C.-Z.; Zhang, Q. Toward Safe Lithium Metal Anode in Rechargeable Batteries: A Review. *Chem. Rev.* **2017**, *117*, 10403−10473.
(3) Wood, K. N.; Noked, M.; Dasgupta, N. P. Lithium Metal Anodes: Toward an Improved Understanding of Coupled Morphological, Electrochemical, and Mechanical Behavior. *ACS Energy Lett.* **2017**, *2*, 664−672.
(4) Trahey, L.; Brushett, F. R.; Balsara, N. P.; Ceder, G.; Cheng, L.; Chiang, Y.-M.; Hahn, N. T.; Ingram, B. J.; Minteer, S. D.; Moore, J. S.; Mueller, K. T.; Nazar, L. F.; Persson, K. A.; Siegel, D. J.; Xu, K.; Zavadil, K. R.; Srinivasan, V.; Crabtree, G. W. Energy Storage Emerging: A Perspective from the Joint Center for Energy Storage Research. *Proc. Natl. Acad. Sci. U. S. A* **2020**, *117*, 12550−12557.
(5) Brandell, D.; Mindemark, J.; Hernandez, G.*Polymer-based Solid State Batteries*; De Gruyter: 2021.
(6) Schulze, M. W.; McIntosh, L. D.; Hillmyer, M. A.; Lodge, T. P. High-Modulus, High-Conductivity Nanostructured Polymer Electrolyte Membranes via Polymerization-Induced Phase Separation. *Nano Lett.* **2014**, *14*, 122−126.
(7) Morris, M. A.; Sung, S. H.; Ketkar, P. M.; Dura, J. A.; Nieuwendaal, R. C.; Epps, T. H., III Enhanced Conductivity via Homopolymer-Rich Pathways in Block Polymer-Blended Electrolytes. *Macromolecules* **2019**, *52*, 9682−9692.
(8) Ketkar, P. M.; Epps, T. H. Nanostructured Block Polymer Electrolytes: Tailoring Self-Assembly to Unlock the Potential in Lithium-Ion Batteries. *Acc. Chem. Res.* **2021**, *54*, 4342−4353.
(9) Ketkar, P. M.; Shen, K.-H.; Fan, M.; Hall, L. M.; Epps, T. H. III. Quantifying the Effects of Monomer Segment Distributions on Ion Transport in Tapered Block Copolymer Electrolytes. *Macromolecules* **2021**, *54*, 7590−7602.
(10) Majewski, P. W.; Gopinadhan, M.; Osuji, C. O. The Effects of Magnatic ield Alignment on Lithium Ion Transport in a Polymer Electrolyte Membrane with Lamellar Morphology. *Polymers* **2019**, *11*, 887.
(11) Schauser, N. S.; Grzetic, D. J.; Tabassum, T.; Kliegle, G. A.; Le, M. L.; Susca, E. M.; Antoine, S.; Keller, T. J.; Delaney, K. T.; Han, S.; Seshadri, R.; Fredrickson, G. H.; Segalman, R. A. The Role of Backbone Polarity on Aggregation and Conduction of Ions in Polymer Electrolytes. *J. Am. Chem. Soc.* **2020**, *142*, 7055−7065.
(12) Borodin, O.; Smith, G. D. Mechanism of Ion Transport in Amorphous Poly(Ethylene Oxide)/LiTFSI from Molecular Dynamics Simulations. *Macromolecules* **2006**, *39*, 1620−1629.
(13) Webb, M. A.; Jung, Y.; Pesko, D. M.; Savoie, B. M.; Yamamoto, U.; Coates, G. W.; Balsara, N. P.; Wang, Z.-G.; Miller, T. F. Systematic Computational and Experimental Investigation of Lithium-Ion Transport Mechanisms in Polyester-Based Polymer Electrolytes. *ACS Cent. Sci.* **2015**, *1*, 198−205.
(14) Choo, Y.; Halat, D. M.; Villaluenga, I.; Timachova, K.; Balsara, N. P. Diffusion and Migration in Polymer Electrolytes. *Prog. Polym. Sci.* **2020**, *103*, 101220.
(15) Xie, S.; Lodge, T. P. Phase Behavior of Binary Polymer Blends Doped with Salt. *Macromolecules* **2018**, *51*, 266−274.
(16) Pesko, D. M.; Timachova, K.; Bhattacharya, R.; Smith, M. C.; Villaluenga, I.; Newman, J.; Balsara, N. P. Neagtive Transference Numbers in Poly(ethylene oxide) Based Eelctrolytes. *J. Electrochem. Soc.* **2017**, *164*, No. E3569.

(17) Evans, J.; Vincent, C. A.; Bruce, P. G. Electrochemical Measurement of Transference Number in Polymer Electrolytes. *Polymer* **1987**, *28*, 2324−2328.
(18) Watanabe, M.; Nagano, S.; Sanui, K.; Ogata, N. Estimation of Li^+ Transport Number in Polymer Electrolytes by the Combination of Complex Impedance and Potentiostatic Polarization Measurements. *Solid State Ion* **1988**, *28*−*30*, 911−917.
(19) Balsara, N. P.; Newman, J. Relationship between Steady-State Current in Symmetric Cells and Transference Number of Electrolytes Comprising Univalent and Multivalent Ions. *J. Electrochem. Soc.* **2015**, *162*, A2720.
(20) Pesko, D. M.; Sawhney, S.; Newman, J.; Balsara, N. P. Comparing Two Electrochemical Approaches for Measuring Transference Numbers in Concentrated Electrolytes. *J. Electrochem. Soc.* **2018**, *165*, A3014.
(21) Gao, K. W.; Fang, C.; Halat, D. M.; Mistry, A.; Newman, J.; Balsara, N. P. The Transference Number. *Energy Environ. Mater.* **2022**, *5*, 1−4.
(22) Sudoh, T.; Shigenobu, K.; Dokko, K.; Watanabe, M.; Ueno, K. Li^+ Transference Number and Dynamic Ion Correlations in Glyme-Li Salt Solvate Ionic Liquids Dilute with Molecular Solvents. *Phys. Chem. Chem. Phys.* **2022**, *24*, 14269−14276.
(23) Shao, Y.; Gudla, H.; Brandell, D.; Zhang, C. Transference Number in Polymer Electrolytes: Mind the Reference-Frame Gap. *J. Am. Chem. Soc.* **2022**, *144*, 7583−7587.
(24) Fong, K. D.; Self, J.; McCloskey, B. D.; Persson, K. A. Onsager Transport Coefficients and Transference Numbers in Polyelectrolyte Solutions and Polymerized Ionic Liquids. *Macromolecules* **2020**, *53*, 9503−9512.
(25) Jones, S. D.; Nguyen, H.; Richardson, P. M.; Chen, Y.-Q.; Wyckoff, K. E.; Hawker, C. J.; Clement, R. J.; Fredrickson, G. H.; Segalman, R. A. Design of Polymeric Zwitterionic Solid Electrolytes with Superionic Lithium Transport. *ACS Cent. Sci.* **2022**, *8*, 169−175.
(26) Galluzzo, M. D.; Maslyn, J. A.; Shah, D. B.; Balsara, N. P. Ohm's Law for Ion Conduction in Lithium and Beyond-Lithium Battery Electrolytes. *J. Chem. Phys.* **2019**, *151*, 020901.
(27) Porcarelli, L.; Gerbaldi, C.; Bella, F.; Nair, J. R. Super Soft All-Ethylene Oxide Polymer Electrolyte for Safe All-Solid Lithium Batteries. *Sci. Rep.* **2016**, *6*, 19892.
(28) Zhang, W.; Nie, J.; Li, F.; Wang, Z. L.; Sun, C. A Durable and Safe Solid-State Lithium Battery with a Hybrid Electrolyte Membrane. *Nano Energy* **2018**, *45*, 413−419.
(29) Zheng, Q.; Pesko, D. M.; Savoie, B. M.; Timachova, K.; Hasan, A. L.; Smith, M. C.; Miller, T. F.; Coates, G. W.; Balsara, N. P. Optimizing Ion Transport in Polyether-Based Electrolytes for Lithium Batteries. *Macromolecules* **2018**, *51*, 2847−2858.
(30) Xu, K. Nonaqueous Liquid Electrolytes for Lithium-Based Rechargeable Batteries. *Chem. Rev.* **2004**, *104*, 4303−4417.
(31) Dahbi, M.; Ghamouss, F.; Tran-Van, F.; Lemordant, D.; Anouti, M. Comparative Study of EC/DMC LiTFSI and $LiPF_6$ Electrolytes for Electrochemical Storage. *J. Power Sources* **2011**, *196*, 9743−9750.
(32) Snyder, R. L.; Choo, Y.; Gao, K. W.; Halat, D. M.; Abel, B. A.; Sundararaman, S.; Prendergast, D.; Reimer, J. A.; Balsara, N. P.; Coates, G. W. Improved Li^+ Transport in Polyacetal Eelctrolytes: Conductivity and Current Fraction in a Series of Polymers. *ACS Energy Lett.* **2021**, *6*, 1886−1891.
(33) Gao, K. W.; Loo, W. S.; Snyder, R. L.; Abel, B. A.; Choo, Y.; Lee, A.; Teixeira, S. C. M.; Garetz, B. A.; Coates, G. W.; Balsara, N. P. Miscible Polyether/Poly(ether-acetal) Electrolyte Blends. *Macromolecules* **2020**, *53*, 5728−5739.
(34) Yu, X. Y.; Xiao, M.; Wang, S. J.; Zhao, Q. Q.; Meng, Y. Z. Fabrication and Characterization of PEO/PPC Polymer Eelectrolyte for Lithium-Ion Battery. *J. Appl. Polym. Sci.* **2010**, *115*, 2718−2722.
(35) Wheatle, B. K.; Lynd, N. A.; Ganesan, V. Effect of Host Incompatibility and Polarity Contrast on Ion Transport in Ternary Polymer-Polymer-Salt Blend Eelctrolytes. *Macromolecules* **2020**, *53*, 875−884.
(36) Caradant, L.; Verdier, N.; Foran, G.; Lepage, D.; Prebe, A.; Ayme-Perrot, D.; Dolle, M. Extrusion of Polymer Blend Electrolytes for Solid-State Lithium Batteries: A Study of Polar Functional Groups. *ACS Appl. Polym. Mater.* **2021**, *3*, 6694−6704.
(37) Blatt, M. P.; Hallinan, D. T. Polymer Blend Electrolytes for Batteries and Beyond. *Ind. Eng. Chem. Res.* **2021**, *60*, 17303−17327.
(38) Loo, W. S.; Mongcopa, K. I.; Gribble, D. A.; Faraone, A. A.; Balsara, N. P. Investigating the Effect of Added Salt on the Chain Dimensions of Poly(Ethylene Oxide) through Small-Angle Neutron Scattering. *Macromolecules* **2019**, *52*, 8724−8732.
(39) Glinka, C. J.; Barker, J. G.; Hammouda, B.; Krueger, S.; Moyer, J. J.; Orts, W. J. The 30 m Small-Angle Neutron Scattering Instruments at the National Institute of Standards and Technology. *J. Appl. Crystallogr.* **1998**, *31*, 430−445.
(40) Kline, S. R. Reduction and Analysis of SANS and USANS Data Using IGOR Pro. *J. Appl. Crystallogr.* **2006**, *39*, 895−900.
(41) Kline, S.SANS Data Reduction Tutorial; NIST Center for Neutron Research. 2001.
(42) Heller, W. T.; Cuneo, M.; Debeer-Schmitt, L.; Do, C.; He, L.; Heroux, L.; Littrell, K.; Pingali, S. V.; Qian, S.; Stanley, C.; Urban, V. S.; Wu, B.; Bras, W. The Suite of Small-Angle Neutron Scattering Instruments at Oak Ridge National Laboratory. *J. Appl. Crystallogr.* **2018**, *51*, 242−248.
(43) Heller, W. T.; Hetrick, J.; Bilheux, J.; Calvo, J. M. B.; Chen, W.-R.; Debeer-Schmitt, L.; Do, C.; Doucet, M.; Fitzsimmons, M. R.; Godoy, W. F.; Granroth, G. E.; Hahn, S.; He, L.; Islam, F.; Lin, J.; Littrell, K. C.; McDonnell, M.; McGaha, J.; Peterson, P. F.; Pingali, S. V.; Qian, S.; Savici, A. T.; Shang, Y.; Stanley, C. B.; Urban, V. S.; Whitfield, R. E.; Zhang, C.; Zhou, w.; Billings, J. J.; Cuneo, M. J.; Leal, R. M. F.; Wang, T.; Wu, B. Drtsans: The Data Reduction Toolkit for Small-Angle Neutron Scattering at Oak Ridge National Laboratory. *SoftwareX* **2022**, *19*, 101101.
(44) Gao, K. W.; Jiang, X.; Hoffman, Z. J.; Sethi, G. K.; Chakraborty, S.; Villaluenga, I.; Balsara, N. P. Optimizing the Monomer Structure of Polyhedral Oligomeric Silsesquioxane for Ion Transport in Hybrid Organic−Inorganic Block Copolymers. *J. Polym. Sci.* **2020**, *58*, 363−371.
(45) Mark, J. E. In *Physical Properties of Polymers Handbook*, 2nd ed.; Eitouni, H. B., Balsara, N. P., Eds.; Springer: New York, 2007; pp 339−356.
(46) Knychała, P.; Timachova, K.; Banaszak, M.; Balsara, N. P. 50th Anniversary Perspective: Phase Behavior of Polymer Solutions and Blends. *Macromolecules* **2017**, *50*, 3051−3065.
(47) Qiu, J.; Mongcopa, K. I.; Han, R.; Lopez-Barron, C. R.; Robertson, M. L.; Krishnamoorti, R. Thermodynamic Interactions in a Model Polydiene/Polyolefin Blend Based on 1,2-Polybutadiene. *Macromolecules* **2018**, *51*, 3107−3115.
(48) Triolo, A.; Lo Celso, F.; Arrighi, V.; Strunz, P.; Lechner, R. E.; Mastragostino, M.; Passerini, S.; Annis, B. K.; Triolo, R. Structural and dynamical characterization of melt PEO−salt mixtures. *Phys. A: Stat. Mech. Appl.* **2002**, *304*, 308−313.
(49) Fullerton-Shirey, S. K.; Maranas, J. K. Effect of LiClO4 on the Structure and Mobility of PEO-Based Solid Polymer Electrolytes. *Macromolecules* **2009**, *42*, 2142−2156.
(50) Xie, S.; Zhang, B.; Mao, Y.; He, L.; Hong, K.; Bates, F. S.; Lodge, T. P. Influence of Added Salt on Chain Conformations in Poly(ethylene oxide) Melts: SANS Analysis with Complications. *Macromolecules* **2020**, *53*, 7141−7149.
(51) Flory, P. J. Thermodynamics of High Polymer Solutions. *J. Chem. Phys.* **1942**, *10*, 51−61.
(52) Huggins, M. L. Some Properties of Solutions of Long-Chain Compounds. *J. Phys. Chem.* **1942**, *46*, 151−158.
(53) Teran, A. A.; Balsara, N. P. Thermodynamics of block copolymers with and without salt. *J. Phys. Chem. B* **2014**, *118*, 4−17.
(54) Loo, W. S.; Balsara, N. P. Organizing Thermodynamic Data Obtained from Multicomponent Polymer Electrolytes: Salt-Containing Polymer Blends and Block Copolymers. *J. Polym. Sci., Part B: Polym. Phys.* **2019**, *57*, 1177−1187.
(55) Hou, K. J.; Loo, W.; Balsara, N. P.; Qin, J. Comparing Experimental Phase Behavior of Ion-Doped Block Copolymers with

https://doi.org/10.1021/acs.macromol.2c01724
Macromolecules 2022, 55, 11023−11033

Theoretical Predictions Based on Selective Ion Solvation. *Macromolecules* **2020**, *53*, 3956−3966.
(56) Nakamura, I.; Wang, Z.-G. Salt-Doped Block Copolymers: Ion Distribution, Domain Spacing and Effective χ parameter. *Soft Matter* **2012**, *8*, 9356−9367.
(57) Dubner, W. S.; Schultz, J. M.; Wignall, G. D. Estimation of Incoherent Backgrounds in SANS Studies of Polymers. *J. Appl. Crystallogr.* **1990**, *23*, 469−475.
(58) Balsara, N. P.; Lohse, D. J.; Graessley, W. W.; Krishnamoorti, R. Small-Angle Neutron Scattering by Partially Deuterated Polymers and Their Blends. *J. Chem. Phys.* **1994**, *100*, 3905−3910.
(59) de Gennes, P. G.*Scaling Concepts in Polymer Chemistry*; Cornell University Press: Ithaca, NY, 1979.
(60) Balsara, N. P.; Fetters, L. J.; Hadjichristidis, N.; Lohse, D. J.; Han, C. C.; Graessley, W. W.; Krishnamoorti, R. Thermodynamic Interactions in Model Polyolefin Blends Obtained by Small-Angle Neutron Scattering. *Macromolecules* **1992**, *25*, 6137−6147.
(61) Akcasu, A. Z.; Tombakoglu, M. Dynamics of Copolymer and Homopolymer Mixtures in Bulk and in Solution via the Random Phase Approximation. *Macromolecules* **1990**, *23*, 607−612.
(62) Benoit, H.; Benmouna, M.; Wu, W.-L. Static Scattering from Multicomponent Polymer and Copolymer Systems. *Macromolecules* **1990**, *23*, 1511−1517.
(63) Hammouda, B. Random Phase Approximation for Compressible Polymer Blends. *J. Non-Cryst. Solids* **1994**, *172*−*174*, 927−931.
(64) Bates, F. S.; Fredrickson, G. H. Block Copolymer Thermodynamics: Theory And Experiment. *Annu. Rev. Phys. Chem.* **1990**, *41*, 525−557.
(65) Wang, Z.-G. Effects of Ion Solvation on the Miscibility of Blend Polymer Blends. *J. Phys. Chem. B* **2008**, *112*, 16205−16213.
(66) Marko, J. F.; Rabin, Y. Microphase Separation of Charged Diblock Copolymers: Melts and Solutions. *Macromolecules* **1992**, *25*, 1503−1509.

Recommended by ACS

Molecular Origin of High Cation Transference in Mixtures of Poly(pentyl malonate) and Lithium Salt
Chao Fang, Rui Wang, *et al.*
APRIL 21, 2023
ACS MACRO LETTERS
READ

Li⁺ Conduction in Glass-Forming Single-Ion Conducting Polymer Electrolytes with and without Ion Clusters
Jiacheng Liu and Jennifer L. Schaefer
MARCH 16, 2023
MACROMOLECULES
READ

Ionic Association in CH_3–$(CH_2$–$CF_2)_n$–CH_3(PVDF)–Li^+–$(CF_3SO_2)_2N^-$ for $n = 1, 4$: A Computational Approach
Mathew Daniel, Nilesh R. Dhumal, *et al.*
FEBRUARY 15, 2022
ACS OMEGA
READ

Structural and Transport Properties of Novel High-Transference Number Electrolytes Based on Perfluoropolyether-*block*-Poly(ethylene oxide) for Applica...
Maryam Molashahi, Behnam Ghalami Choobar, *et al.*
NOVEMBER 16, 2022
MACROMOLECULES
READ

Get More Suggestions >

https://doi.org/10.1021/acs.macromol.2c01724
Macromolecules 2022, 55, 11023−11033